PLOS COMPUTATIONAL BIOLOGY

RESEARCH ARTICLE

A low-threshold potassium current enhances sparseness and reliability in a model of avian auditory cortex

Margot C. Bjoring[1], **C. Daniel Meliza**[1,2]*

1 Department of Psychology, University of Virginia, Charlottesville, VA, USA, **2** Neuroscience Graduate Program, University of Virginia, Charlottesville, VA, USA

* cdm8j@virginia.edu

OPEN ACCESS

Citation: Bjoring MC, Meliza CD (2019) A low-threshold potassium current enhances sparseness and reliability in a model of avian auditory cortex. PLoS Comput Biol 15(1): e1006723. https://doi.org/10.1371/journal.pcbi.1006723

Editor: Arthur Leblois, Centre National de la Recherche Scientifique, FRANCE

Received: August 15, 2018

Accepted: December 17, 2018

Published: January 28, 2019

Data Availability Statement: All stimuli and data files have been deposited in Data Dryad (doi:10.5061/dryad.js11601) and are publically available.

Funding: This work received funding from the Thomas F. and Kate Miller Jeffress Memorial Trust, Bank of America, N.A., Trustee (CDM; https://hria.org/tmf/jeffress/) and the National Science Foundation Graduate Research Fellowship Program (MCB; https://www.nsfgrfp.org/). The funders had no role in study design, data collection and analysis, decision to publish, or preparation of the manuscript.

Abstract

Birdsong is a complex vocal communication signal, and like humans, birds need to discriminate between similar sequences of sound with different meanings. The caudal mesopallium (CM) is a cortical-level auditory area implicated in song discrimination. CM neurons respond sparsely to conspecific song and are tolerant of production variability. Intracellular recordings in CM have identified a diversity of intrinsic membrane dynamics, which could contribute to the emergence of these higher-order functional properties. We investigated this hypothesis using a novel linear-dynamical cascade model that incorporated detailed biophysical dynamics to simulate auditory responses to birdsong. Neuron models that included a low-threshold potassium current present in a subset of CM neurons showed increased selectivity and coding efficiency relative to models without this current. These results demonstrate the impact of intrinsic dynamics on sensory coding and the importance of including the biophysical characteristics of neural populations in simulation studies.

Author summary

Maintaining a stable mental representation of an object is an important task for sensory systems, requiring both recognizing the features required for identification and ignoring incidental changes in its presentation. The prevailing explanation for these processes emphasizes precise sets of connections between neurons that capture only the essential features of an object. However, the intrinsic dynamics of the neurons themselves, which determine how these inputs are transformed into spiking outputs, may also contribute to the neural computations underlying object recognition. To understand how intrinsic dynamics contribute to sensory coding, we constructed a computational model capable of simulating a neural response to an auditory stimulus using a detailed description of different intrinsic dynamics in a higher-order avian auditory area. The results of our simulation showed that intrinsic dynamics can have a profound effect on processes underlying object recognition. These findings challenge the view that patterns of connectivity alone account for the emergence of stable object representations and encourage greater consideration of the functional implications of the diversity of neurons in the brain.

Competing interests: The authors have declared that no competing interests exist.

Introduction

Vocal communication requires an auditory system that can reliably classify signals. For example, in human speech, phonemes produced by different speakers and in different contexts vary broadly in acoustic structure. Despite this, they are perceived as discrete, invariant categories [1], even when boundaries between phonemes are exceptionally sharp, as with the approximately 10 ms difference in voice-onset time that separates the English phonemes /d/ and /t/ [2]. Categorization of vocal signals is not limited to human speech perception; many other species that communicate vocally show similar abilities [3–6].

As in other sensory systems, categorical responses to auditory objects emerge in higher-order areas of the cortex [7–12]. Neurons in these areas are characterized by a high degree of selectivity, or sparseness, in their responses to exemplars from different categories [13, 14], as well as tolerance, or invariance, in their responses to exemplars of the same category [15]. Similar properties are observed in the responses of secondary auditory areas in humans to phonemes [16–18]. However, in spite of a substantial body of theoretical work [19–21], the circuit and cellular mechanisms underlying the emergence of categorical responses remains poorly understood.

Songbirds communicate with acoustically complex vocalizations, which requires them to perform many of the same kinds of auditory discrimination tasks as humans [22]. In the avian auditory system, the caudal mesopallium (CM) is a cortical-level area that contains a population of neurons highly selective for particular song elements, yet tolerant of low-level acoustic differences between renditions [8, 10]. In contrast, the neurons in Field L, immediately upstream of CM, show low selectivity and tolerance [23]. In the classical model of selectivity, complex feature representations emerge through feedforward synaptic connections that pool sparsely from upstream sources [24]. This model does not match experimental evidence from CM, however, which shows that selective neurons receive a more distributed pool of inputs than the sparse model would predict [25]. A distributed scheme of selectivity could arise from nonlinear dynamics within the neurons themselves, but the mechanisms of this have not been explored.

In many of the auditory areas in the hindbrain and midbrain, nonlinear neural dynamics profoundly affect how a variety of low-level acoustic features are encoded [26–28]. For example, neurons that express a low-threshold potassium current ($I_{K_{LT}}$) produce highly phasic responses, responding to rapid increases in excitation but not to slow or steady-state depolarizations [29, 30]. These dynamics are critical to temporal precision in sound localization circuits [28, 31] and can enhance signal detection in noisy conditions [32]. Could intrinsic dynamics also contribute to sensory processing at cortical levels? In CM, the putatively excitatory neurons exhibit diverse intrinsic firing patterns [33]. About 30% exclusively produce phasic responses that depend on a low-threshold potassium current, whereas the remainder produce mostly tonic responses. The functional significance of this diversity remains unclear.

The goal of the present study is to understand how $I_{K_{LT}}$ and the phasic dynamics it produces could contribute to the emergence of selectivity and tolerance in CM. To investigate how intrinsic dynamics could interact with sensory-driven inputs, we developed an auditory response model that combines a spectrotemporal receptive field (RF) with a biophysical spike generation mechanism. In this linear-dynamical cascade model, the RF component approximates the integration over multiple spectral channels and time lags performed by the circuits upstream of the neuron and by the neuron's dendritic tree. This part of the model is identical to the linear filter component of the classic linear-nonlinear Poisson (LNP) model [34, 35]. However, instead of using the output of the filter as the conditional intensity of a probabilistic spiking process, we feed it into a single-compartment, biophysical model that produces spikes

through Hodgkin-Huxley dynamics. Using this approach, which allows us to integrate our knowledge about intracellular properties in CM into a model for high-level coding properties, we found that $I_{K_{LT}}$ enhances selectivity and robustness to noise.

Results

Fig 1A represents the operation of the linear-dynamical cascade model. The spectrogram of a zebra finch song stimulus was convolved with the RF to produce a driving current $I_{stim}(t)$, which was injected into a single-compartment dynamical neuron model containing several voltage-dependent sodium and potassium currents. The mathematical descriptions of these currents were derived from an intracellular study of the excitatory neurons in the caudal mesopallium (CM) of zebra finches [33], and the RFs are drawn from parameterized features of zebra finch field L neurons [36]. A key feature of this model is that it can produce phasic or tonic responses depending on the conductance of a low-threshold potassium current ($g_{K_{LT}}$), which is experimentally known to be present in some CM neurons. Variability in the responses of the model was generated with the addition of the $I_{noise}(t)$ current. This current adds random

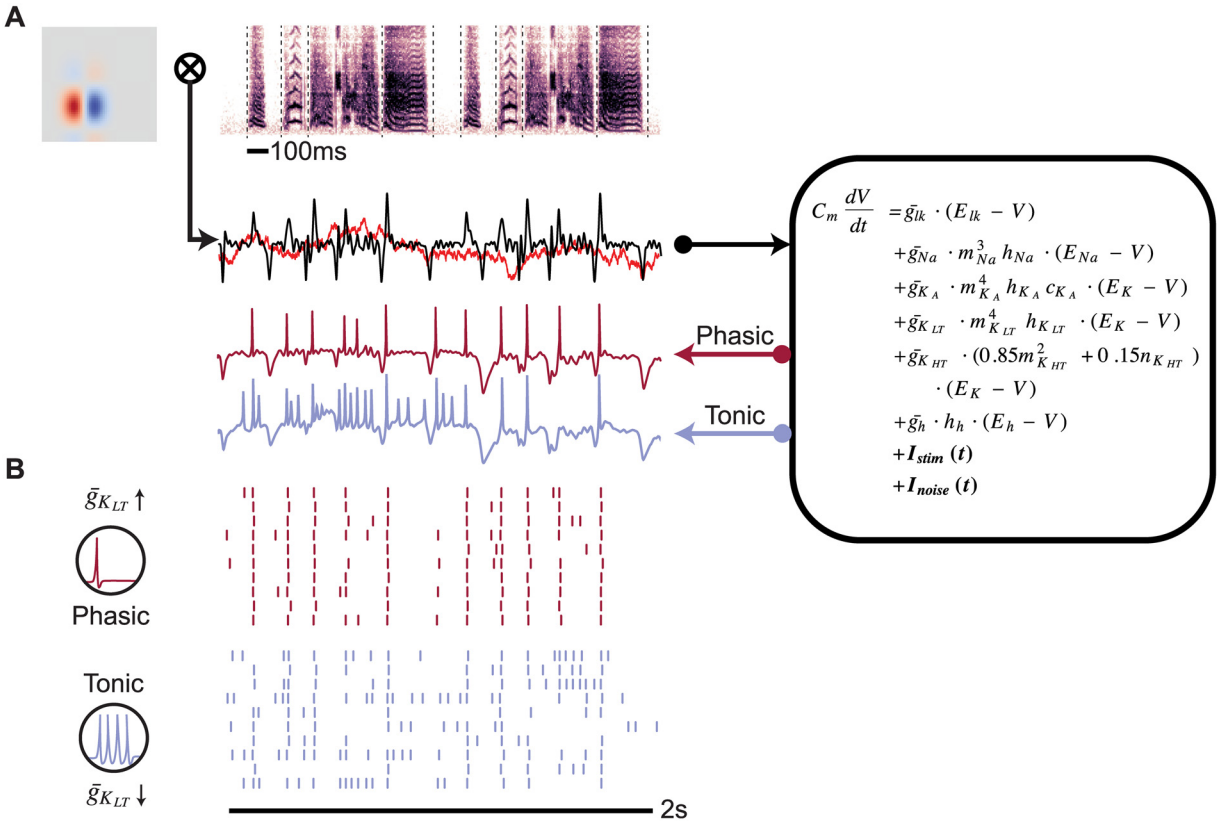

Fig 1. Simulating auditory responses with biophysical dynamics. (A) Auditory responses were simulated by convolving a spectrotemporal receptive field (upper left) with the spectrogram (upper right) of an auditory stimulus, in this case a zebra finch song. Black dashed lines indicate syllable boundaries. The resulting convolution (black line) provided the driving current ($I_{stim}(t)$) to the single-compartment biophysical model used in this study (right). Red noise (bright red line) was added in each trial as a stimulus-independent current ($I_{noise}(t)$) with SNR of 4. The model was integrated to produce a simulated voltage trace (lower left). The conductance of a low-threshold potassium channel parameter ($g_{K_{LT}}$) was set to 0 nS for tonic dynamics (blue line) or 50 nS for phasic dynamics (dark red line). Voltage traces are vertically offset for better visibility. (B) Raster plots of the full simulation for the stimulus-RF pair in A across 10 trials for phasic (red) and tonic (blue) model. The example demonstrates how the phasic model produces more reliable and temporally precise responses than the tonic model.

https://doi.org/10.1371/journal.pcbi.1006723.g001

noise with a $1/f^2$ power spectrum (red noise), which approximates the statistics of spontaneous synaptic noise *in vivo* [37], at a signal-to-noise ratio (SNR) of four.

As seen in Fig 1B, the model's intrinsic dynamics affected its response to zebra finch song. When $g_{K_{LT}}$ was high (phasic model), responses were more precise and more reliable than when $g_{K_{LT}}$ was absent (tonic model). This effect was consistent across RFs with different spectral and temporal parameters and across multiple stimuli (Fig 2). It is important to note that although $I_{K_{LT}}$ is an outward current with an overall hyperpolarizing influence, increasing it did not simply reduce excitability. In some cases, the phasic model responded at a much lower rate and to only a handful of notes across the stimulus set (Fig 2B). In other cases, the firing rates of the phasic and tonic models were nearly the same (Fig 2A and 2C), and the effects of manipulating $g_{K_{LT}}$ were primarily on trial-to-trial variability. Overall, the average difference in firing rate between tonic and phasic models was significant but small and highly variable (0.36 ± 0.36 Hz; $t_{59} = 7.74$; $p < 0.001$).

To investigate how phasic excitability affects functional response properties, in this study we focused on rate-based theories of sensory coding. The fundamental idea of rate coding is that neurons convey information about sensory inputs by modulating their average firing rate over relatively long intervals. Following previous studies [10, 38], we defined these intervals by dividing the responses into segments corresponding to song syllables (as in Fig 1), which are well-defined units of zebra finch song that convey information about individual identity [39]. We then calculated metrics based on how the average rates within those intervals were distributed across syllables and trials (Fig 3A).

We first examined whether phasic dynamics made neurons more selective. Selectivity, also known as lifetime sparseness, is a well-established rate-coding metric defined as the tendency of a neuron to respond strongly to only a small subset of stimuli [13]. A selective neuron has a

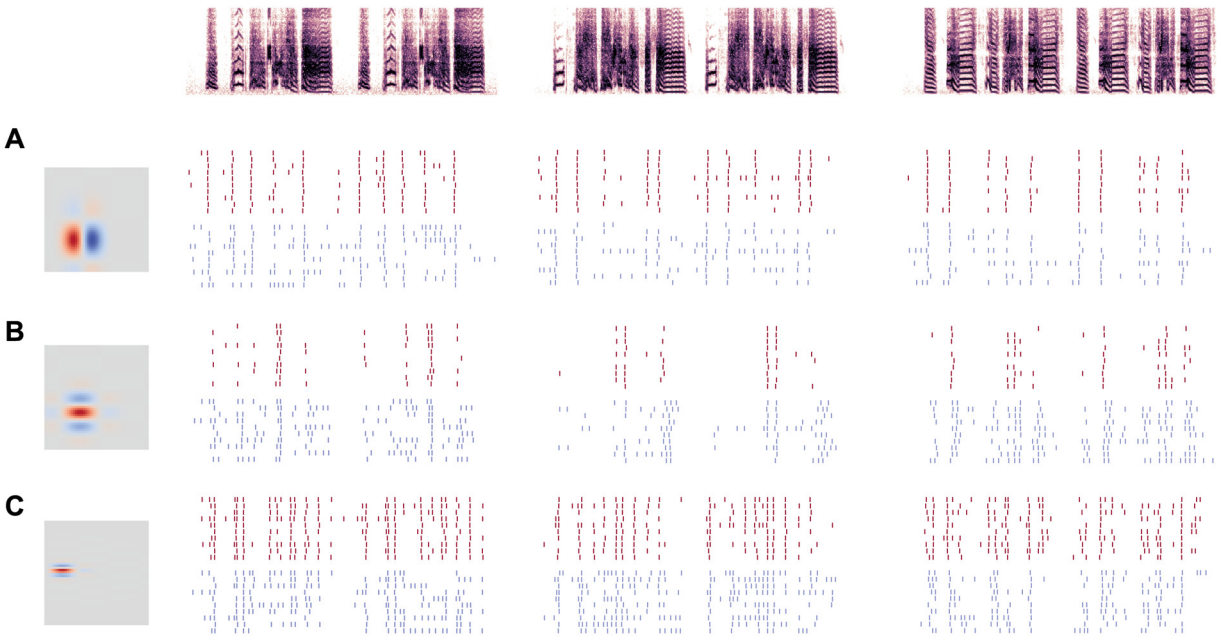

Fig 2. Responses of simulated neurons. Raster plots for models with three different RFs (rows, A—C) in response to three different stimuli (columns). As in Fig 1, raster plots show 10 simulated responses of models with phasic (red) or tonic (blue) dynamics. Different RFs produce different levels of sparseness, selectivity, and precision in the spiking responses, but tonic models are consistently less precise and less selective than phasic models.

https://doi.org/10.1371/journal.pcbi.1006723.g002

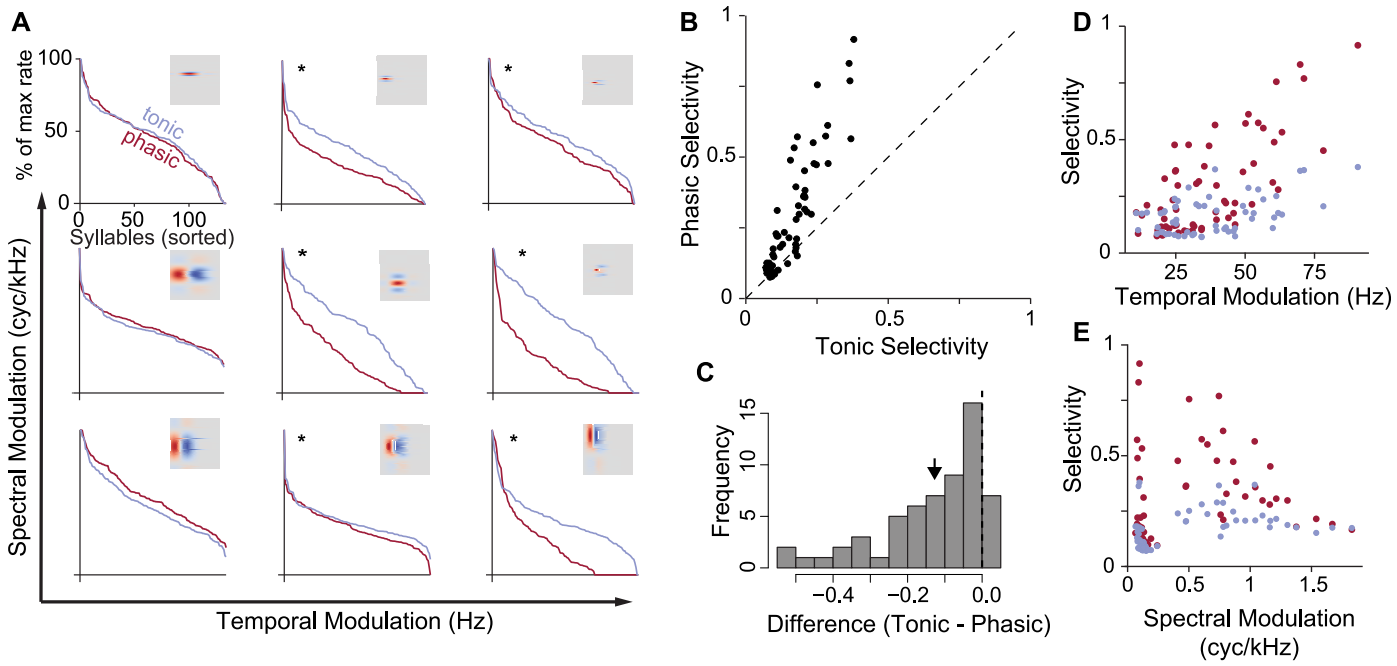

Fig 3. Phasic dynamics increase selectivity. (A) Normalized cumulative distribution of response rates for nine example RFs with phasic (red) and tonic (blue) dynamics. High selectivity is indicated by a response distribution with a heavy tail on the left side of the plot, indicating that only a few stimuli account for the strongest responses. Asterisks indicate a significant difference in the distribution of response rates ($p < 0.05$, Komolgorov-Smirnov test). Receptive fields are arranged by increasing spectral and temporal modulation frequency. (B) Selectivity of paired phasic and tonic models. Selectivity is quantified using activity fraction (see Methods). Each point corresponds to one RF. The dashed reference line indicates the line of equal selectivity. Models with phasic dynamics are consistently more selective than their tonic counterparts ($t_{59} = -7.18$; $p < 0.001$). (C) Histogram of the difference in selectivity between phasic and tonic models. Negative values indicate the phasic model has higher selectivity than the tonic model. The black arrow shows the mean difference. (D) Selectivity and the effects of intrinsic dynamics increase with the temporal modulation frequency of the RFs (red; $F_{1,116} = 27$; $p < 0.001$). (E) In contrast, there is not a significant interaction between spectral modulation frequency and intrinsic dynamics ($F_{1,116} = 0.001$; $p = 0.97$), and the main effect of spectral modulation frequency on selectivity is not clear.

https://doi.org/10.1371/journal.pcbi.1006723.g003

skewed, heavy-tailed response distribution in which a few stimuli account for the strongest responses, and the remainder produce only weak excitation. In contrast, a less selective neuron has a small-tailed, Gaussian response distribution, with most of the responses concentrated around the mean. For the examples shown in Fig 3A, the models with phasic dynamics tended to be significantly more selective than the corresponding models with tonic dynamics. This effect was not uniform, but appeared to be stronger in the models with higher temporal-modulation frequencies in their RFs.

The effects highlighted in these examples were also seen in a larger set of simulations with 60 different RFs, which were matched to the distribution of spectral and temporal parameters seen in the zebra finch auditory cortex [36]. Each RF was combined with phasic and tonic dynamics for a total of 120 models. Across this population, phasic models were consistently more selective than tonic models with the same RFs (Fig 3B and 3C), and the effects of intrinsic dynamics were larger for models with higher temporal modulation (Fig 3D).

We also observed that phasic models were more reliable across trials, indicating that they were less affected by the noise current I_{noise}. To quantify this effect in the context of rate coding, we calculated the mutual information (MI) between the response rate and syllable identity. MI is defined as the difference between the response (total) entropy, which represents how much information the neuron can carry based on its range of firing rates, and noise (or conditional) entropy, which represents how much information is lost due to the variability of a

neuron's response to the same stimulus. A neuron that responds more similarly across trials will have a low noise entropy, bringing its MI closer to its total entropy.

Fig 4 illustrates how intrinsic dynamics affected the distribution of response rates across trials for the same nine example RFs shown previously. The tonic models tended to have a higher total entropy across these examples, although in several cases, the phasic models are slightly higher. However, for all of these examples, the response rates of the phasic models cluster more closely around the mean response, resulting in lower noise entropy compared to the tonic models.

Across all 60 RF pairs, the total entropy was slightly higher for tonic neurons (Fig 5A and 5B). That advantage was more than canceled out by a much larger increase in noise entropy (Fig 5C and 5D). Every phasic simulation had lower noise entropy than its tonic pair. The net effect was that phasic models had higher MI than the corresponding tonic models (Fig 5E and 5F).

In the data described above, the noise current had a $1/f^2$ spectral distribution (red noise), which is thought to approximate how spontaneous synaptic currents are dominated by low-frequency fluctuations [37]. The total amplitude of the noise was set so that the inter-trial variations in firing patterns resembled what has been reported in extracellular recordings [23, 36, 40]. To test whether the results were robust to these assumptions, we varied the amplitude and spectral distribution of the noise current. As would be expected, selectivity and mutual information decreased overall as signal-to-noise ratio (SNR) decreased (Fig 6A–6D). However, at each SNR value tested, the phasic models consistently had lower noise entropy and higher MI and selectivity. We also found that the same pattern of results was seen when the noise current had a $1/f$ distribution, which is less dominated by low-frequency fluctuations but is also considered to be biologically valid [41]. In contrast, when the noise had a flat frequency distribution (white noise), the effects of intrinsic dynamics were not significant (Fig 6E–6H).

As a further test of parameter sensitivity, we compared results across a wide range of values for $g_{K_{LT}}$, which determines the magnitude of the low-threshold potassium current that causes phasic firing. As shown previously [33, 42], increasing $g_{K_{LT}}$ over a narrow range leads to a dramatic change in firing patterns: once the low-threshold current is strong enough to counteract voltage-gated sodium currents, it becomes nearly impossible for the neuron to fire more than one action potential in response to a step current. This may explain the bimodal distribution of firing properties in CM [33]. The phasic and tonic dynamical models examined here represent these two modes, but it is likely that the distribution of $g_{K_{LT}}$ varies more broadly. Interestingly, we did not see any evidence of a switch-like change in encoding properties as we varied $g_{K_{LT}}$ over the range encompassed by the two exemplar models (Fig 6I–6L). Increasing $g_{K_{LT}}$ instead produced nearly linear increases in selectivity and mutual information, and linear decreases in total and noise entropy.

How are selectivity and MI related? In these simulations, total entropy and selectivity were negatively correlated (Fig 7A). This effect is unsurprising given that selective neurons respond similarly to a large proportion of stimuli. They encode more information about a few stimuli at the expense of encoding less information about the entire stimulus set. However, when we consider coding efficiency, which quantifies how much of this potential bandwidth is actually used instead of being lost to noise (Fig 7C), two trends emerge. First, tonic models have lower coding efficiency than phasic models, consistent with the observation that they have higher noise entropy and lower MI. Second, only phasic neurons are able to achieve both high selectivity and high coding efficiency.

As an independent test of the validity of this model, we applied the same selectivity and MI analyses to a public corpus of recordings from zebra finch CM [43]. The relationships between

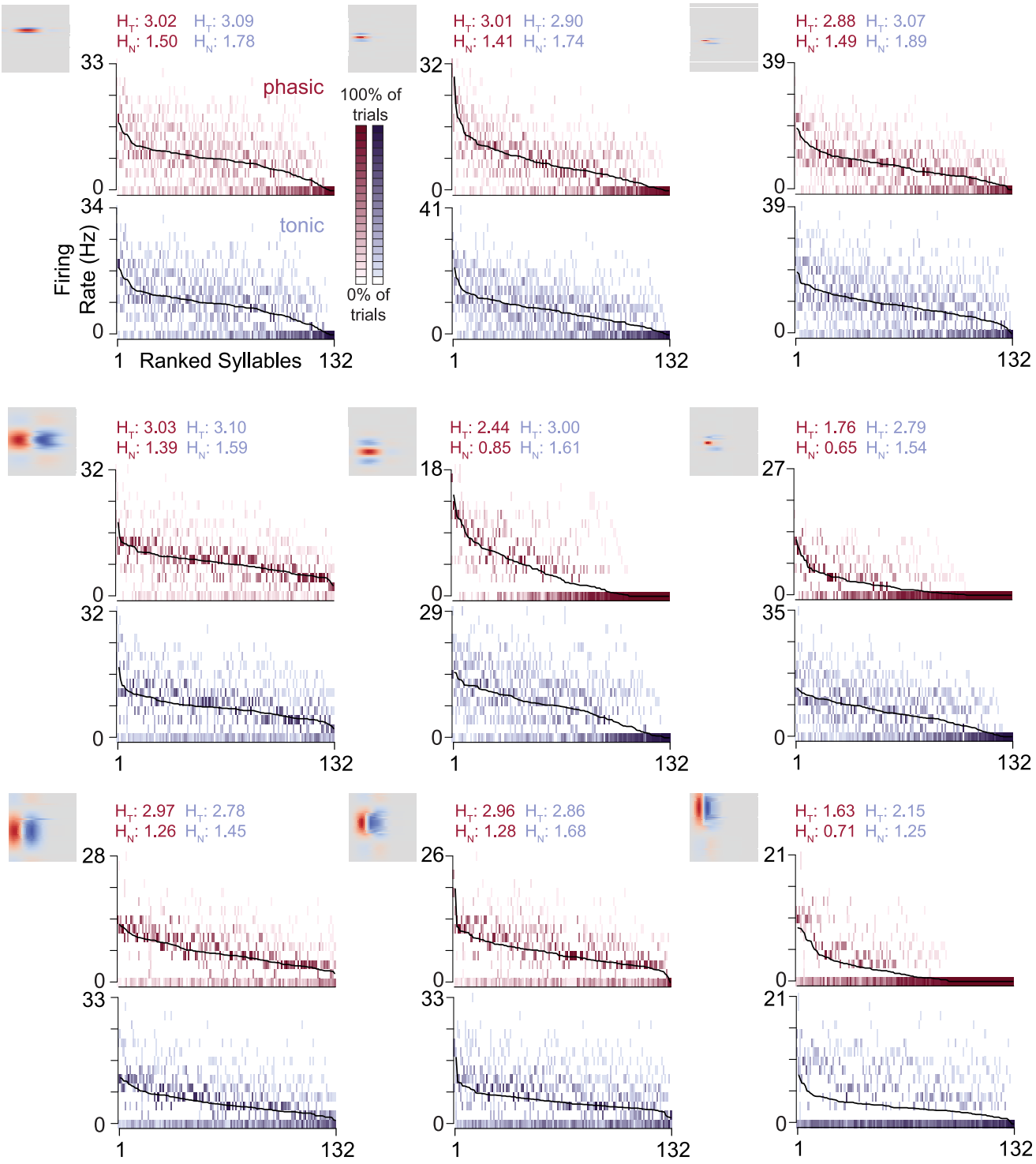

Fig 4. Phasic dynamics reduce trial-to-trial variability in spike rates. Full response distributions for the nine example neurons shown previously. Response rates are calculated for each syllable and trial and discretized into 15 bins. The black lines indicate the average across trials; the spread of response rate bins around those lines show the trial-to-trial variability of the response rates. Darker colors indicate that response rates to the given syllable fall within that bin more frequently. Response distributions where the bins close to the mean line are dark and the bins further away are light, *e.g.* the phasic example in the top row, middle column, have low trial-to-trial variability. Distributions with darker scatter further away from the mean, such as the paired tonic example, have higher trial-to-trial variability. Overall, the phasic examples were less variable than their paired tonic models. Total entropy (H_T) and noise entropy (H_N) values are shown above each plot (phasic: red; tonic: blue).

https://doi.org/10.1371/journal.pcbi.1006723.g004

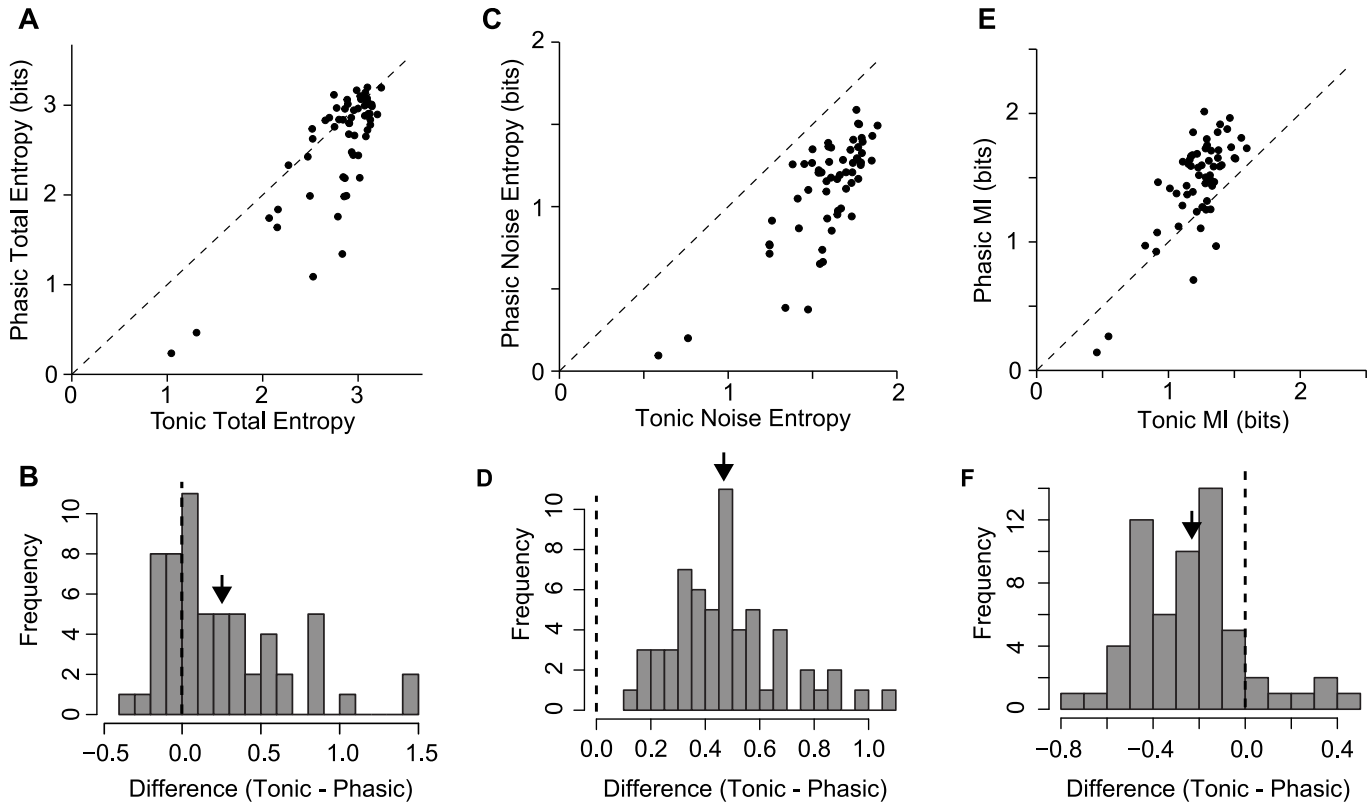

Fig 5. Phasic dynamics confer increased mutual information about syllable identity by increasing reliability. (A) Comparison of total (response) entropy, which represents the maximum information capacity of the model. Phasic and tonic models had similar total entropy, though tonic models had a slight advantage ($t_{59} = 4.70$; $p < 0.001$). (B) Histogram of the difference in total entropy between phasic and tonic models. Positive values indicate the tonic model had higher total entropy than the phasic model. (C) Comparison of noise entropy, which represents variation in responses to the same stimulus across trials. Noise entropy decreases the amount of information conveyed from the theoretical maximum. All of the phasic models had lower noise entropy than tonic models ($t_{59} = 18.10$; $p < 0.001$). (D) Histogram of the difference in noise entropy between phasic and tonic models. (E) Mutual information of paired phasic and tonic models. On average, models with phasic dynamics had higher mutual information than the corresponding tonic models ($t_{59} = -7.40$; $p = 0.02$). (F) Histogram of the difference in mutual information between phasic and tonic models.

https://doi.org/10.1371/journal.pcbi.1006723.g005

selectivity and MI predicted by the model were largely borne out in the experimental data. We observed a similar tradeoff between selectivity and total entropy (Fig 7B), and an even stronger positive correlation between selectivity and coding efficiency (Fig 7D). The average coding efficiency was lower in the experimental data, which likely reflects additional sources of variability *in vivo*. Selectivity was somewhat higher *in vivo*, perhaps because of additional nonlinearities in the actual CM receptive fields. Interestingly, the cluster of models with high coding efficiency and low selectivity seen in the simulated data is not present in the experimental data.

Why are models with phasic dynamics consistently more reliable and selective than models with tonic dynamics? Low-threshold potassium currents counteract the regenerative sodium current produced during spike initiation. As a result, cells expressing these currents only spike in response to a rapid increase in excitation. These dynamics enable phasic neurons in the auditory hindbrain and midbrain to detect coherent excitation with high temporal precision, even in noisy conditions [32, 44, 45]. Consistent with this idea, we observed in our sensory model that moments of high concordance between the RF and the stimulus created peaks in the driving current $I_{stim}(t)$. The phasic models spiked almost exclusively at these moments

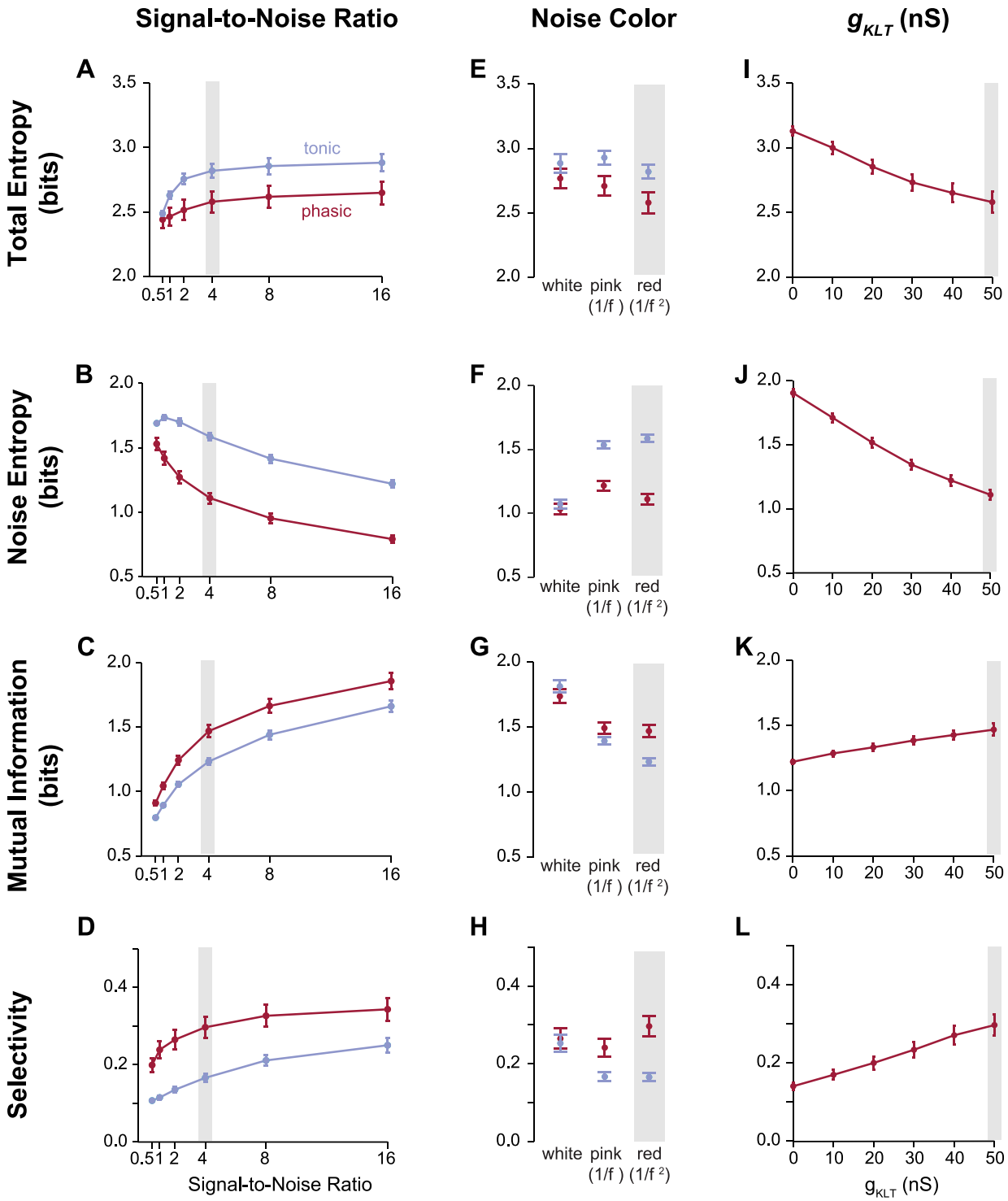

Fig 6. The effect of phasic dynamics are robust to noise statistics and linearly related to $g_{K_{LT}}$ expression. (A—D) The effect of varying signal-to-noise ratios (SNR) on the outcome of the total entropy (A), noise entropy (B), MI (C), and selectivity (D) analyses. As the amplitude of the noise current increases relative to the amplitude of the stimulus-driven current (decreasing SNR), noise increases and MI and selectivity decrease, but phasic models continue to outperform tonic models. The red lines shows the means of phasic models, and the blue line shows the means of tonic models. Bars show standard error. The gray boxes indicate the parameter values used in this study. (E—H) The effect of noise shapes on total entropy (E), noise entropy (F), MI (G), and selectivity (H). Adding white noise erases the advantage of phasic neurons, but white noise is biologically unrealistic and ineffective at driving significant amounts of variability (F). More biologically realistic noise shapes with greater power at low frequencies, such as pink ($1/f$) and red ($1/f^2$), produce comparable results when SNR is adjusted to match variability. Mean and standard

error shown. White noise shown at SNR 0.5, pink noise at SNR 2, and red noise at SNR 4. (I–L) The effect of $g_{K_{LT}}$ conductance on total entropy (I), noise entropy (J), MI (K), and selectivity (L) for the phasic models.

https://doi.org/10.1371/journal.pcbi.1006723.g006

(Fig 8A). In contrast, the tonic models were more sensitive to the absolute level of $V(t)$ and increased their firing rate as the integral of $I_{stim}(t)$ became more positive (Fig 8B).

Based on this observation and the positive correlation between selectivity and temporal modulation frequency (Fig 3D), we hypothesized that the effect of phasic excitability on selectivity would be stronger when the RF produced a driving current with sparse peaks of excitation. In the spectral domain, this corresponds to convolutions that have more power at higher frequencies and RFs that have higher temporal modulation frequencies. To test this effect specifically, we simulated another set of data with eight RFs, holding all RF parameters constant except temporal modulation (Ω_t), which we varied between 10 and 80 Hz.

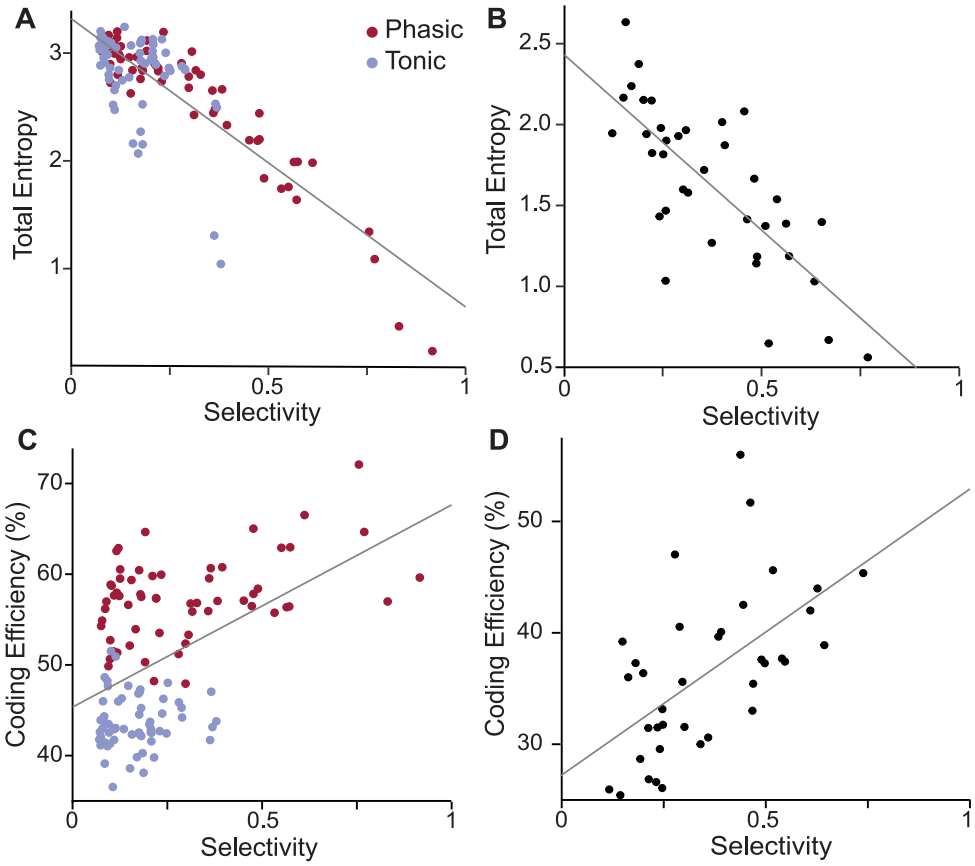

Fig 7. The model predicts a relationship between coding efficiency and selectivity. (A) Total entropy and selectivity are negatively correlated for both phasic and tonic models, showing the inherent trade-off between selectivity and entropy (Pearson $r = -0.84$; $p < 0.001$). (B) CM neurons in zebra finches exhibit the same trade-off (Pearson $r = -0.76$; $p < 0.001$). Data from Theunissen *et al.* [43]. (C) Coding efficiency, calculated as the percentage of total entropy not lost to noise, is enhanced by phasic dynamics. Tonic models (blue points) cluster around lower values of coding efficiency and also lack the population of high selectivity neurons that the phasic models (red points) exhibit. The population of models show a moderate positive correlation between coding efficiency and selectivity (Pearson $r = 0.48$; $p < 0.001$). (D) CM neurons in zebra finches show a strong positive correlation between selectivity and coding efficiency (Pearson $r = 0.58$; $p < 0.001$), as they lack the population of low-selectivity, high-reliability neurons seen in the model (C). Data from Theunissen *et al.* [43].

https://doi.org/10.1371/journal.pcbi.1006723.g007

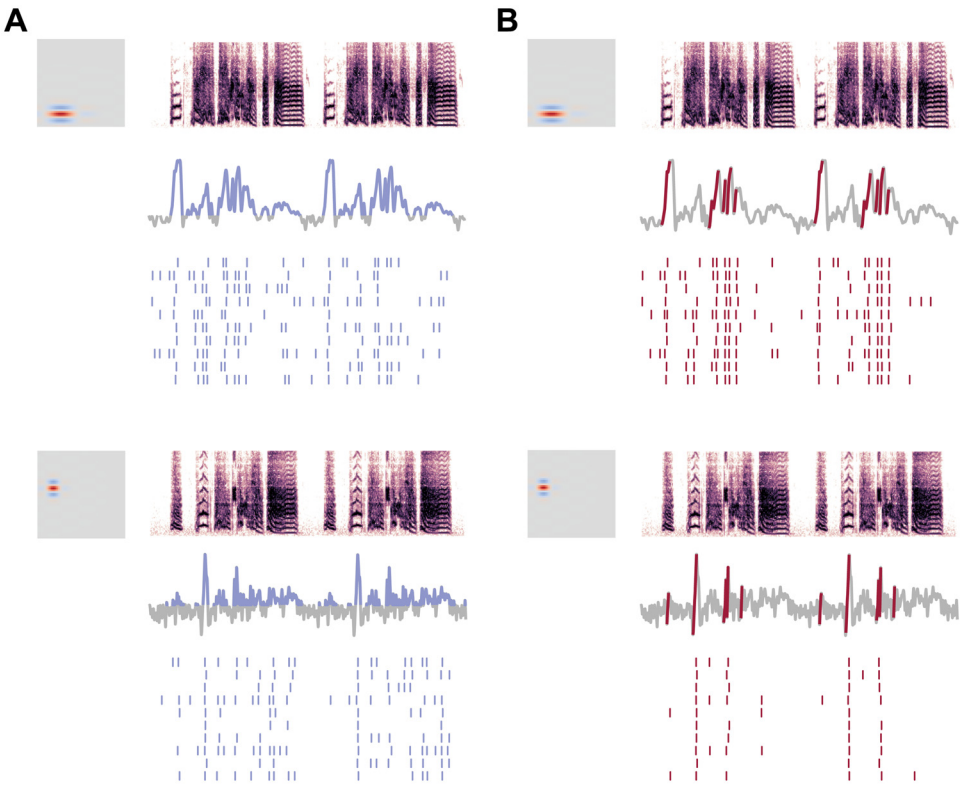

Fig 8. Phasic selectivity is driven by slope detection. (A) Tonic models responded to the level of excitation in the driving current. Spiking activity aligned well to the moments when net excitation was greater than zero, and the model produced jittery, unreliable responses to broad peaks of excitation. Blue segments of the trace mark when the convolution is positive. (B) Phasic models responded primarily when driving current contained a positive slope with a high rate of change. Spike times aligned well to these slopes. The red segments of the convolution mark the times at which the difference of the smoothed convolution was 1.5 standard deviations above the mean difference. Because such slopes were relatively scarce and brief, the spikes predicted by the phasic model were selective and had little temporal variation.

https://doi.org/10.1371/journal.pcbi.1006723.g008

At low values of Ω_t, convolutions of the RF and a stimulus produced mostly slow modulations, and the response of phasic and tonic models were similar, as the example in Fig 9A shows. As the modulations in the convolution became faster and large deflections became sparser (Fig 9A, 80 Hz), the response of the phasic model became more selective, while the tonic model, responding to the shape of the slow modulation still present in the signal, showed no inclination toward selectivity. Fig 9B presents the full set of simulations, showing a strong interaction between the temporal modulation of the RF and selectivity. Phasic models showed a strong increase in selectivity as Ω_t of the RF increased, but tonic models were unaffected.

Discussion

This study investigated how intrinsic dynamics could contribute to the emergence of selectivity and tolerance in CM, a cortical-level auditory area. We used a novel linear-dynamical cascade model that combines a spectrotemporal receptive field with a biophysical description of intrinsic membrane dynamics. We found that a low-threshold potassium current ($I_{K_{LT}}$) strongly affected how the model neurons encoded information about song stimuli in firing rates. Phasic models (with high $I_{K_{LT}}$) were more selective and more tolerant of noise than models with identical RFs and tonic dynamics. Furthermore, a population of phasic and tonic

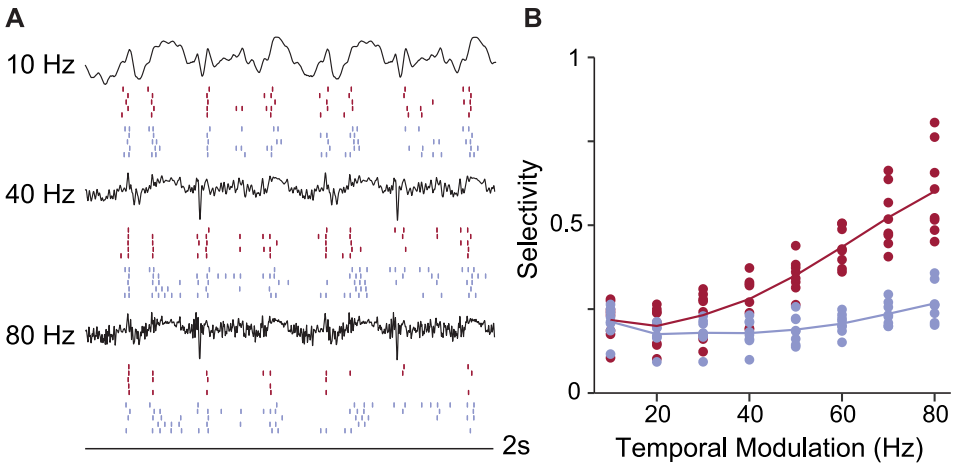

Fig 9. Selectivity depends on an interaction between phasicness and RF shape. (A) Example convolutions of an RF with Ω_t = 10, 40, and 80 Hz. Rasters of phasic (red) and tonic (blue) responses for 5 of 10 trials are shown below. At 10 Hz, slow modulations predominate. At 40 Hz, the convolution contains more sharp peaks. At 80 Hz, the peaks become sparser, but only the response of the phasic example becomes more selective. (B) The selectivity of neural simulations increases as the temporal modulation of the RF (Ω_t) increases, but only for phasic models. The selectivity of tonic simulations shows little effect. The interaction between model type and Ω_t is significant ($F_{1,124} = 93$; $p < 0.001$).

https://doi.org/10.1371/journal.pcbi.1006723.g009

models reproduced the distribution of selectivity and coding efficiency seen *in vivo* (Fig 7). These results suggest that a diversity of intrinsic intracellular properties contributes to the higher-order functional properties seen in CM.

The model we developed for this analysis is a special case of the linear-nonlinear (LN) cascade model used in many studies of sensory coding [46–48]. In the standard LN model, the nonlinearity is a history-independent function that transforms the output of the linear stage into an instantaneous spiking probability. More recent LN models incorporate history dependence through a linear kernel convolved with past spike times, as in the generalized linear model [35, 49], or through non-biological, dynamical state variables, as in the spike response and generalized integrate-and-fire models [50–52]. The present study required a more biologically realistic representation of the dynamics so that we could manipulate a specific current of interest, $I_{K_{LT}}$. We therefore used a conductance-based biophysical model to generate spikes. This model lacks many of the morphological and physiological properties of CM neurons and omits any circuit-level organization, but it is capable of reproducing the tonic and phasic firing patterns observed in CM slices [33].

For the linear stage of the model, we used simplified STRFs from a previous study of Field L [36], which is the primary source of ascending auditory input to CM [53]. The reason we did not use STRFs from CM is that linear RF estimates from this area have poor predictive power [40] and are therefore unlikely to be representative of the true synaptic tuning. As seen in another secondary auditory area, the caudomedial nidopallium [54], RFs in CM may involve nonlinear combinations of multiple feature vectors. These nonlinearities may reflect local excitatory and inhibitory circuitry, and as methods for estimating parameters in these more complex models improve [55], it will be important to also consider the contributions of intrinsic dynamics. Here, we chose to use a simplified, parametric RF model so that we could systematically investigate how different RF features interacted with nonlinear dynamics. The clear effects seen here with simplified RFs argue that intrinsic dynamics have the potential to facilitate categorical responses even in the absence of complex circuitry.

Our main finding is that increased $I_{K_{LT}}$ caused responses to conspecific song to become sparser, more precise, and more reliable (Fig 2). We focused here on quantifying these effects using several well-established rate-based encoding metrics [10, 38], though the effects on temporal precision are worthy of future consideration. Selectivity, which is also called activity fraction or lifetime sparseness [13, 14], was strongly enhanced by $I_{K_{LT}}$ (Fig 3). Syllables that produced strong responses remained strong, but weak responses became weaker, causing response rate distributions to become more heavy-tailed. This led to a reduction in the total entropy of the distributions (Fig 5), which reflects the fact that a more selective neuron responds similarly to all the weak stimuli and therefore encodes little information about the majority of the stimulus set. At the same time, the phasic models lost much less of their bandwidth to noise, which led to a net increase in mutual information and coding efficiency. Thus, $I_{K_{LT}}$ can increase both the sparseness of the neural code and its reliability.

The effects of $I_{K_{LT}}$ were not simply a product of reduced excitability. Rather, they arose from complex interactions between the RF, the stimulus, and the nonlinear dynamics of the membrane. Phasic dynamics resulted in larger increases in selectivity when RFs were tuned to rapid temporal modulations. Because zebra finch song has strong, broadband rhythmic structure, these RFs produced convolutions with brief peaks of excitation (Figs 8 and 9) [36]. Phasic dynamics also had stronger effects for realistic noise currents that were dominated by low-frequency fluctuations (Fig 6E–6H) [37, 41]. Together, these results indicate that $I_{K_{LT}}$ enables neurons to reliably pick out brief moments of strong excitation against a background of low-frequency noise. This is consistent with extensive theoretical and experimental studies of $I_{K_{LT}}$ in the auditory hindbrain and midbrain [29, 56–59].

Although these results provide strong support for the possibility that intrinsic dynamics are relevant to neural encoding in zebra finch CM, they do not rule out the contribution of synaptic mechanisms. Indeed, strong feedforward inhibition sharpens selectivity and increases temporal precision in cortical-level rodent and avian auditory areas [60–63] in a manner similar to the effects produced by $I_{K_{LT}}$ in this study. Further work is needed to determine if the cell-intrinsic effects of $I_{K_{LT}}$ are replicating the effects of feedforward inhibition, albeit in a more compact way, or if there are more consequential differences between these mechanisms.

This study shows that phasic dynamics can enhance selectivity and tolerance for conspecific song, which raises the question of why CM contains both tonic and phasic neurons. The functional significance of diverse intrinsic dynamics has been examined in a variety of brain areas. In the olfactory bulb, diverse dynamics in mitral cells help to decorrelate responses across neurons [64]; in the visual thalamus, bursting in neurons that project to the cortex enhances signal-to-noise ratios [65]; and in the electrosensory lateral line lobe, bursting dynamics provide a parallel information stream for low-frequency events [66]. In CM, some neurons are strongly selective and others are not [8, 10, 67], and a similar pattern is also seen in mammalian secondary auditory areas [15, 68]. Although we can only speculate at this point as to the behavioral significance, our data indicate that diversity in the intrinsic dynamics of CM neurons may contribute substantially to the functional diversity. The models in this study sampled from a distribution of RFs with a broad range of spectral and temporal statistics, but only when the population included both phasic and tonic dynamics did we observe the broad, correlated distribution of selectivity and coding efficiency seen in zebra finch CM (Fig 7). Interestingly, the model response properties were more diverse than seen *in vivo*, suggesting that $I_{K_{LT}}$ may be selectively expressed in a subset of neurons, such as the ones tuned to rapid temporal modulations.

Animals from a broad range of species are able to perform invariant auditory object recognition in challenging conditions [69–72]. In many sensory pathways, there is a hierarchical increase in selectivity and tolerance for natural objects that is thought to underlie this remarkable ability. However, the circuit-level implementation of this computation remains largely theoretical [73]. Although many models have followed Hubel and Wiesel [24] in focusing on how excitatory and inhibitory connectivity enables neurons to aggregate inputs tuned to simpler features, the nonlinear mechanisms of spike generation, which determine how these inputs are summed, are also thought to be important [74]. The present study supports this idea by showing how a single voltage-gated current, $I_{K_{LT}}$, has the potential to dramatically shift how information about stimulus identity is encoded. As we become increasingly aware of the diversity of cell types in the brain [75–77] and the activity-dependent mechanisms that can modulate intrinsic electrophysiological properties [78–80], it is important to account for intrinsic dynamics in models of sensory processing.

Materials and methods

Linear-dynamical cascade model

Biophysical model. The model used in this study is a conductance-based, single-compartment model for CM neurons [33], which was adapted from the ventral cochlear nucleus model of Rothman and Manis [29]. The currents in the model include four voltage-gated potassium and sodium currents, a leak current, and a hyperpolarization-activated cation current. A key component of the model is the low-threshold potassium current ($I_{K_{LT}}$), which determines whether the neuron produces tonic or phasic responses to step depolarization. When $g_{K_{LT}}$ (the maximal conductance of $I_{K_{LT}}$) is low, the model neuron produces sustained responses to weak and moderate depolarizations; when $g_{K_{LT}}$ is high, the model only fires phasically, at the onset of the current step. The model parameter values follow Rothman and Manis [29], with a few adjustments to match the resting potential and spike threshold for CM neurons. The calculations presented here used the consensus model parameters from Chen and Meliza [33] for tonic and phasic cells (Table 1). S1 Appendix. contains the full model specification. The model simulation code was generated using spyks (https://github.com/melizalab/spyks; version 0.6.6), and the dynamics were integrated using a 5th-order Runge-Kutta algorithm with an adaptive error tolerance of 1×10^{-5} and an interpolated step size of 0.025 ms.

Table 1. Parameter values for the tonic and phasic models.

Parameter	Tonic	Phasic
C	**60 pF**	**40 pF**
g_{lk}	1.3 nS	1.3 nS
E_{lk}	−75 mV	−75 mV
g_{Na}	750 nS	750 nS
E_{Na}	55 mV	55 mV
g_{K_A}	30 nS	30 nS
$g_{K_{HT}}$	95 nS	95 nS
$g_{K_{LT}}$	**0 nS**	**50 nS**
E_K	−82 mV	−82 mV
g_h	0.5 nS	0.5 nS
E_h	−43 mV	−43 mV

Bolded values differ between the tonic and phasic models.

https://doi.org/10.1371/journal.pcbi.1006723.t001

Auditory response simulation. To simulate an auditory response, the model was driven by a current, $I_{stim}(t)$, which was calculated from the convolution of a spectrotemporal receptive field (RF) with the spectrogram of an auditory stimulus. In this formulation, the RF approximated the synaptic drive to the neuron as a weighted sum of linear, time-invariant filters over different frequency channels. To simulate stimulus-independent variability in the response, a second driving current, $I_{noise}(t)$, was added. The noise current was randomly generated red noise ($1/f^2$ power spectrum) scaled relative to the signal to achieve a set signal-to-noise ratio (SNR). Red noise was chosen for its power at low frequencies which efficiently drives response variability in the neuron models and for the biological validity of the power spectrum of the noise. $1/f^{\alpha}$ spectra are found in many complex, natural systems including the brain [41], and the statistics of synaptic noise are well approximated by a $1/f^2$ spectrum [37]. For all of the analyses presented in this paper with the exception of the analysis of the effect of the signal-to-noise ratio, SNR was set at 4.

RFs were constructed with a Gabor filter based on Woolley *et al.* [36]:

$$\begin{aligned} \mathrm{RF}(t,f) &= H(t)\cdot G(f), \\ H(t) &= e^{-0.5[(t-t_0)/\sigma_t]^2}\cdot\cos(2\pi\cdot\Omega_t(t-t_0)+P_t), \\ G(f) &= e^{-0.5[(f-f_0)/\sigma_f]^2}\cdot\cos(2\pi\cdot\Omega_f(f-f_0)), \end{aligned}$$

where H is the temporal dimension of the RF, G is the spectral dimension of the RF, t_0 is the latency, f_0 is the peak frequency, σ_t and σ_f are the temporal and spectral bandwidths, Ω_t and Ω_f are the temporal and spectral modulation frequencies, and P_t is the temporal phase. Parameter values were randomly drawn from distributions set to match the modulation transfer function (MTF) of the RF ensemble to the MTF of zebra finch song [36, 81]. The integral of each RF was normalized to one.

The models' responses were simulated using 30 zebra finch songs recorded from our colony. Each recording was comprised of a single song motif repeated twice. Recordings were normalized to the same RMS amplitude and edited to be 2.025 s long, with 50 ms of microphone noise at the beginning to pad the convolution, and scaled to a consistent RMS amplitude. Start and end times of syllables were identified by visual inspection. Repeated syllables were grouped in the decoding analyses. Spectrograms of the stimuli were calculated using the short-time Fourier transform algorithm with a Hanning window of 256 points and then resampled to give a frequency resolution of 50 channels between 0 and 8 kHz. Successive windows were spaced 1.0 ms apart.

In the context of this simulation, a model neuron was defined as the combination of one RF and one biophysical parameter set (phasic or tonic). 60 RFs were generated to produce paired phasic and tonic simulations (n = 120 neurons or 60 pairs). For the analysis of the relationship between selectivity and temporal modulation, 8 RFs were generated and for each RF Ω_t was set to 10, 20, . . ., 80 (n = 128 neurons or 8 sets of pairs). The 30 zebra finch songs were presented 10 times each to each neuron with different values of $I_{noise}(t)$ producing trial-to-trial variability. Noise currents in each trial were identical between paired phasic and tonic neurons. The total amplitude of the convolution was normalized by the bandwidth of the RF on the frequency axis (σ_f) to account for the differences in amplitudes between narrowband and broadband RFs. The output of the model was a simulated voltage trace.

The stimuli and simulated responses have been deposited with Data Dryad (doi:10.5061/dryad.js11601).

Data analysis. Spike times were extracted from the simulated responses using a simple window discriminator (https://github.com/melizalab/quickspikes; version 1.3.3). We calculated spike rate, $r_{i,j}$, as the number of spikes evoked by syllable i in trial j, divided by the

duration of the syllable. Selectivity was quantified using activity fraction [10, 13], a nonparametric index defined as:

$$A = \frac{1 - (\sum r_i/N)^2 / \sum r_i^2/N}{1 - 1/N}$$

where r_i is the rate for syllable i averaged across trials, and N is the total number of syllables.

Mutual information (MI), total entropy, and noise entropy were calculated following Jeanne *et al.* [38]. Response rates were discretized into 15 bins between the minimum and maximum rate of the model. Total entropy was calculated as $H(R) = -\Sigma p(r)\log_2 p(r)$, noise entropy as $H(R|S) = -\Sigma p(s)\Sigma p(r|s)\log_2 p(r|s)$, and mutual information as $I(R;S) = H(R) - H(R|S)$, where r is the rate and s is the syllable. Because of the large number of stimuli and trials, and because we were interested in differences between models presented with exactly the same stimuli, we did not correct entropy or MI for sample size bias. Coding efficiency was calculated as $1 - (H(R|S)/H(R))$.

Stimuli

Thirty male zebra finches provided song recordings that were used as stimuli in the simulation experiments. All animal use was performed in accordance with the Institutional Animal Care and Use Committee of the University of Virginia. Adult zebra finches were obtained from the University of Virginia breeding colony. During recording, zebra finches were housed in a soundproof auditory isolation box (Eckel Industries, Cambridge, MA) with *ad libitum* food and water and were kept on a 16:8h light:dark schedule. A mirror was added to the box to stimulate singing. Recordings were made with an Audio-Technica Pro 70 microphone, digitized with a Focusrite Scarlett 2i2 at 44.1 kHz, and stored to disk using custom C++ software (https://github.com/melizalab/jill; version 2.1.4). A typical recording session lasted 2–3 days. A single representative song was selected from each bird's recorded corpus and was high-pass filtered at 500Hz with a 4th-order Butterworth filter.

Extracellular data

Analyses based on extracellular data were performed on the publicly available dataset from Theunissen *et al.* [43] available at http://crcns.org/data-sets/aa/aa-2. Neural recordings were collected from adult male zebra finches as described in Gill *et al.* [82]. Only responses from CM neurons presented with conspecific song were used for these analyses ($n = 37$). Selectivity and MI analyses were performed as described above, except that 10 response bins were used for MI analysis instead of 15, due to the smaller stimulus set.

Supporting information

S1 Appendix. Model equations.
(PDF)

Acknowledgments

We thank Tyler Robbins for assistance in model development and JC Cang and Alev Erisir for critical comments and discussions.

Author Contributions

Conceptualization: C. Daniel Meliza.

Formal analysis: Margot C. Bjoring.

Methodology: C. Daniel Meliza.

Visualization: Margot C. Bjoring.

Writing – original draft: Margot C. Bjoring.

Writing – review & editing: C. Daniel Meliza.

References

1. Iverson P, Kuhl PK. Perceptual magnet and phoneme boundary effects in speech perception: Do they arise from a common mechanism? Percept Psychophys. 2000; 62(4):874–886. https://doi.org/10.3758/BF03206929 PMID: 10883591
2. Liberman AM, Harris KS, Kinney JA, Lane H. The discrimination of relative onset-time of the components of certain speech and nonspeech patterns. J Exp Psychol. 1961; 61(5):379. https://doi.org/10.1037/h0049038 PMID: 13761868
3. May B, Moody DB, Stebbins WC. Categorical perception of conspecific communication sounds by Japanese macaques, M acacafuscata. JASA. 1989; 85(2):837–847. https://doi.org/10.1121/1.397555
4. Ehret G. Categorical perception of mouse-pup ultrasounds in the temporal domain. Animal Behav. 1992; 43(3):409–416. https://doi.org/10.1016/S0003-3472(05)80101-0
5. Hauser MD, Marler P. Food-associated calls in rhesus macaques (Macaca mulatta): I. Socioecological factors. Behav Ecol. 1993; 4(3):194–205.
6. Elie JE, Theunissen FE. Zebra finches identify individuals using vocal signatures unique to each call type. Nat Commun. 2018; 9(1):4026. https://doi.org/10.1038/s41467-018-06394-9 PMID: 30279497
7. Rauschecker JP, Tian B, Hauser M. Processing of complex sounds in the macaque nonprimary auditory cortex. Science. 1995; 268(5207):111–114. https://doi.org/10.1126/science.7701330 PMID: 7701330
8. Gentner TQ, Margoliash D. Neuronal populations and single cells representing learned auditory objects. Nature. 2003; 424(6949):669–674. https://doi.org/10.1038/nature01731 PMID: 12904792
9. Tsunada J, Lee JH, Cohen YE. Differential representation of auditory categories between cell classes in primate auditory cortex. J Physiol (Lond). 2012; 590(Pt 13):3129–3139. https://doi.org/10.1113/jphysiol.2012.232892
10. Meliza CD, Margoliash D. Emergence of selectivity and tolerance in the avian auditory cortex. J Neurosci. 2012; 32(43):15158–15168. https://doi.org/10.1523/JNEUROSCI.0845-12.2012 PMID: 23100437
11. Elie JE, Theunissen FE. Meaning in the avian auditory cortex: neural representation of communication calls. Eur J Neurosci. 2015; 41(5):546–567. https://doi.org/10.1111/ejn.12812 PMID: 25728175
12. Mouterde SC, Elie JE, Mathevon N, Theunissen FE. Single neurons in the avian auditory cortex encode individual identity and propagation distance in naturally degraded communication calls. J Neurosci. 2017; p. 2220–16.
13. Rolls E, Tovee MJ. Sparseness of the neuronal representation of stimuli in the primate temporal visual cortex. J Neurophysiol. 1995; 73(2):713–726. https://doi.org/10.1152/jn.1995.73.2.713 PMID: 7760130
14. Vinje WE, Gallant JL. Sparse coding and decorrelation in primary visual cortex during natural vision. Science. 2000; 287(5456):1273–1276. https://doi.org/10.1126/science.287.5456.1273 PMID: 10678835
15. Zoccolan D, Kouh M, Poggio T, DiCarlo JJ. Trade-off between object selectivity and tolerance in monkey inferotemporal cortex. J Neurosci. 2007; 27(45):12292–12307. https://doi.org/10.1523/JNEUROSCI.1897-07.2007 PMID: 17989294
16. Chang EF, Rieger JW, Johnson K, Berger MS, Barbaro NM, Knight RT. Categorical speech representation in human superior temporal gyrus. Nat Neurosci. 2010; 13(11):1428–1432. https://doi.org/10.1038/nn.2641 PMID: 20890293
17. Mesgarani N, Cheung C, Johnson K, Chang EF. Phonetic feature encoding in human superior temporal gyrus. Science. 2014; 343(6174):1006–1010. https://doi.org/10.1126/science.1245994 PMID: 24482117
18. de Heer WA, Huth AG, Griffiths TL, Gallant JL, Theunissen FE. The hierarchical cortical organization of human speech processing. J Neurosci. 2017; 37(27):6539–6557. https://doi.org/10.1523/JNEUROSCI.3267-16.2017 PMID: 28588065

19. Riesenhuber M, Poggio T. Models of object recognition. Nat Neurosci. 2000; 3 Suppl(Supp):1199–1204. https://doi.org/10.1038/81479 PMID: 11127838

20. Larson E, Billimoria CP, Sen K. A biologically plausible computational model for auditory object recognition. J Neurophysiol. 2009; 101(1):323–331. https://doi.org/10.1152/jn.90664.2008 PMID: 18987124

21. Bastos AM, Usrey WM, Adams RA, Mangun GR, Fries P, Friston KJ. Canonical microcircuits for predictive coding. Neuron. 2012; 76(4):695–711. https://doi.org/10.1016/j.neuron.2012.10.038 PMID: 23177956

22. Gentner T. Neural systems for individual song recognition in adult birds. Ann N Y Acad Sci. 2004; 1016(1):282–302. https://doi.org/10.1196/annals.1298.008 PMID: 15313781

23. Calabrese A, Woolley SMN. Coding principles of the canonical cortical microcircuit in the avian brain. PNAS. 2015; 112(11):3517–3522. https://doi.org/10.1073/pnas.1408545112 PMID: 25691736

24. Hubel D, Wiesel TN. Receptive fields and functional architecture in two nonstriate visual areas (18 and 19) of the cat. J Neurophysiol. 1965; 28(2):229–289. https://doi.org/10.1152/jn.1965.28.2.229 PMID: 14283058

25. Perks KE, Gentner TQ. Subthreshold membrane responses underlying sparse spiking to natural vocal signals in auditory cortex. Eur J Neurosci. 2015; 41(5):725–733. https://doi.org/10.1111/ejn.12831 PMID: 25728189

26. Carr CE, Soares D. Evolutionary convergence and shared computational principles in the auditory system. Brain Behav Evol. 2002; 59(5-6):294–311. https://doi.org/10.1159/000063565 PMID: 12207085

27. Khurana S, Remme MWH, Rinzel J, Golding NL. Dynamic interaction of Ih and IK-LVA during trains of synaptic potentials in principal neurons of the medial superior olive. J Neurosci. 2011; 31(24):8936–8947. https://doi.org/10.1523/JNEUROSCI.1079-11.2011 PMID: 21677177

28. Gai Y, Kotak VC, Sanes DH, Rinzel J. On the localization of complex sounds: temporal encoding based on input-slope coincidence detection of envelopes. J Neurophysiol. 2014; 112(4):802–813. https://doi.org/10.1152/jn.00044.2013 PMID: 24848460

29. Rothman JS, Manis PB. Differential expression of three distinct potassium currents in the ventral cochlear nucleus. J Neurophysiol. 2003; 89(6):3070–3082. https://doi.org/10.1152/jn.00125.2002 PMID: 12783951

30. Gai Y, Doiron B, Kotak V, Rinzel J. Noise-gated encoding of slow inputs by auditory brain stem neurons with a low-threshold K+ current. J Neurophysiol. 2009; 102(6):3447–3460. https://doi.org/10.1152/jn.00538.2009 PMID: 19812289

31. Carr CE, MacLeod KM. Microseconds matter. PLoS biology. 2010; 8(6):e1000405. https://doi.org/10.1371/journal.pbio.1000405 PMID: 20613856

32. Svirskis G, Kotak V, Sanes DH, Rinzel J. Enhancement of signal-to-noise ratio and phase locking for small inputs by a low-threshold outward current in auditory neurons. J Neurosci. 2002; 22(24):11019–11025. https://doi.org/10.1523/JNEUROSCI.22-24-11019.2002 PMID: 12486197

33. Chen AN, Meliza CD. Phasic and Tonic Cell Types in the Zebra Finch Auditory Caudal Mesopallium. J Neurophysiol. 2018; 119(3):1127–1139. https://doi.org/10.1152/jn.00694.2017 PMID: 29212920

34. Theunissen FE, Sen K, Doupe AJ. Spectral-temporal receptive fields of nonlinear auditory neurons obtained using natural sounds. J Neurosci. 2000; 20(6):2315–2331. https://doi.org/10.1523/JNEUROSCI.20-06-02315.2000 PMID: 10704507

35. Pillow JW, Paninski L, Uzzell VJ, Simoncelli EP, Chichilnisky EJ. Prediction and decoding of retinal ganglion cell responses with a probabilistic spiking model. J Neurosci. 2005; 25(47):11003–11013. https://doi.org/10.1523/JNEUROSCI.3305-05.2005 PMID: 16306413

36. Woolley SMN, Gill PR, Fremouw T, Theunissen FE. Functional groups in the avian auditory system. J Neurosci. 2009; 29(9):2780–2793. https://doi.org/10.1523/JNEUROSCI.2042-08.2009 PMID: 19261874

37. Destexhe A, Rudolph M, Fellous JM, Sejnowski TJ. Fluctuating synaptic conductances recreate in vivo-like activity in neocortical neurons. Neuroscience. 2001; 107(1):13–24. https://doi.org/10.1016/S0306-4522(01)00344-X PMID: 11744242

38. Jeanne JM, Thompson JV, Sharpee TO, Gentner TQ. Emergence of learned categorical representations within an auditory forebrain circuit. J Neurosci. 2011; 31(7):2595–2606. https://doi.org/10.1523/JNEUROSCI.3930-10.2011 PMID: 21325527

39. Cynx J. Experimental determination of a unit of song production in the zebra finch (Taeniopygia guttata). J Comp Psychol. 1990; 104(1):3. https://doi.org/10.1037/0735-7036.104.1.3 PMID: 2354628

40. Sen K, Theunissen FE, Doupe AJ. Feature analysis of natural sounds in the songbird auditory forebrain. J Neurophysiol. 2001; 86(3):1445–1458. https://doi.org/10.1152/jn.2001.86.3.1445 PMID: 11535690

41. Bedard C, Kroeger H, Destexhe A. Does the 1/f frequency scaling of brain signals reflect self-organized critical states? Phys Rev Lett. 2006; 97(11):118102. https://doi.org/10.1103/PhysRevLett.97.118102 PMID: 17025932

42. Rothman JS, Manis PB. The roles potassium currents play in regulating the electrical activity of ventral cochlear nucleus neurons. Journal of Neurophysiology. 2003; 89(6):3097–3113. https://doi.org/10.1152/jn.00127.2002 PMID: 12783953

43. Theunissen FE, Gill P, Noopur A, Zhang J, Woolley SMN, Fremouw T. Single-unit recordings from multiple auditory areas in male zebra finches. CRCNS.org. 2011.

44. Rathouz M, Trussell L. Characterization of outward currents in neurons of the avian nucleus magnocellularis. J Neurophysiol. 1998; 80(6):2824–2835. https://doi.org/10.1152/jn.1998.80.6.2824 PMID: 9862887

45. Khurana S, Liu Z, Lewis AS, Rosa K, Chetkovich D, Golding NL. An essential role for modulation of hyperpolarization-activated current in the development of binaural temporal precision. J Neurosci. 2012; 32(8):2814–2823. https://doi.org/10.1523/JNEUROSCI.3882-11.2012 PMID: 22357864

46. Eggermont JJ, Aertsen A, Johannesma PIM. Quantitative characterisation procedure for auditory neurons based on the spectro-temporal receptive field. Hear Res. 1983; 10(2):167–190 PMID: 6602799

47. Keat J, Reinagel P, Reid RC, Meister M. Predicting every spike: a model for the responses of visual neurons. Neuron. 2001; 30(3):803–817. https://doi.org/10.1016/S0896-6273(01)00322-1 PMID: 11430813

48. Schwartz O, Pillow JW, Rust NC, Simoncelli EP. Spike-triggered neural characterization. J Vis. 2006; 6(4):484–507. https://doi.org/10.1167/6.4.13 PMID: 16889482

49. Paninski L. Maximum likelihood estimation of cascade point-process neural encoding models. Network. 2004; 15(4):243–262. https://doi.org/10.1088/0954-898X_15_4_002 PMID: 15600233

50. Jolivet R, Lewis TJ, Gerstner W. Generalized integrate-and-fire models of neuronal activity approximate spike trains of a detailed model to a high degree of accuracy. J Neurophysiol. 2004; 92(2):959–976. https://doi.org/10.1152/jn.00190.2004 PMID: 15277599

51. Kobayashi R, Tsubo Y, Shinomoto S. Made-to-order spiking neuron model equipped with a multi-time-scale adaptive threshold. Front Comput Neurosci. 2009; 3:9. https://doi.org/10.3389/neuro.10.009.2009 PMID: 19668702

52. Lynch EP, Houghton CJ. Parameter estimation of neuron models using in-vitro and in-vivo electrophysiological data. Front Neuroinform. 2015; 9:10. https://doi.org/10.3389/fninf.2015.00010 PMID: 25941485

53. Vates GE, Broome BM, Mello CV, Nottebohm F. Auditory pathways of caudal telencephalon and their relation to the song system of adult male zebra finches. J Comp Neurol. 1996; 366(4):613–642. https://doi.org/10.1002/(SICI)1096-9861(19960318)366:4<613::AID-CNE5>3.0.CO;2-7 PMID: 8833113

54. Kozlov AS, Gentner TQ. Central auditory neurons have composite receptive fields. PNAS. 2016; 113(5):1441–1446. https://doi.org/10.1073/pnas.1506903113 PMID: 26787894

55. Kaardal JT, Theunissen FE, Sharpee TO. A low-rank method for characterizing high-level neural computations. Front Comput Neurosci. 2017; 11:68. https://doi.org/10.3389/fncom.2017.00068 PMID: 28824408

56. Golding NL, Robertson D, Oertel D. Recordings from slices indicate that octopus cells of the cochlear nucleus detect coincident firing of auditory nerve fibers with temporal precision. J Neurosci. 1995; 15(4):3138–3153. https://doi.org/10.1523/JNEUROSCI.15-04-03138.1995 PMID: 7722652

57. Locke RE, Nerbonne JM. Role of Voltage-Gated K+ Currents in Mediating the Regular-Spiking Phenotype of Callosal-Projecting Rat Visual Cortical Neurons. J Neurophysiol. 1997; 78(5):2321–2335. https://doi.org/10.1152/jn.1997.78.5.2321 PMID: 9356385

58. Sivaramakrishnan S, Oliver DL. Distinct K currents result in physiologically distinct cell types in the inferior colliculus of the rat. J Neurosci. 2001; 21(8):2861–2877. https://doi.org/10.1523/JNEUROSCI.21-08-02861.2001 PMID: 11306638

59. Meng X, Huguet G, Rinzel J. Type III Excitability, Slope Sensitivity and Coincidence Detection. Discrete Contin Dyn Syst Ser A. 2012; 32(8):2729–2757. https://doi.org/10.3934/dcds.2012.32.2729 PMID: 23667306

60. Wehr M, Zador AM. Balanced inhibition underlies tuning and sharpens spike timing in auditory cortex. Nature. 2003; 426(6965):442–446. https://doi.org/10.1038/nature02116 PMID: 14647382

61. Froemke RC, Merzenich MM, Schreiner CE. A synaptic memory trace for cortical receptive field plasticity. Nature. 2007; 450(7168):425–429. https://doi.org/10.1038/nature06289 PMID: 18004384

62. Thompson JV, Jeanne JM, Gentner TQ. Local inhibition modulates learning-dependent song encoding in the songbird auditory cortex. J Neurophysiol. 2013; 109(3):721–733. https://doi.org/10.1152/jn.00262.2012 PMID: 23155175

63. Schneider DM, Woolley SMN. Sparse and background-invariant coding of vocalizations in auditory scenes. Neuron. 2013; 79(1):141–152. https://doi.org/10.1016/j.neuron.2013.04.038 PMID: 23849201

64. Padmanabhan K, Urban NN. Intrinsic biophysical diversity decorrelates neuronal firing while increasing information content. Nat Neurosci. 2010; 13(10):1276–1282. https://doi.org/10.1038/nn.2630 PMID: 20802489

65. Krahe R, Gabbiani F. Burst firing in sensory systems. Nat Rev Neurosci. 2004; 5(1):13. https://doi.org/10.1038/nrn1296 PMID: 14661065

66. Oswald AMM, Chacron MJ, Doiron B, Bastian J, Maler L. Parallel processing of sensory input by bursts and isolated spikes. J Neurosci. 2004; 24(18):4351–4362. https://doi.org/10.1523/JNEUROSCI.0459-04.2004 PMID: 15128849

67. Meliza CD, Chi Z, Margoliash D. Representations of conspecific song by starling secondary forebrain auditory neurons: toward a hierarchical framework. J Neurophysiol. 2010; 103(3):1195–1208. https://doi.org/10.1152/jn.00464.2009 PMID: 20032245

68. Cohen YE. Selectivity for the Spatial and Nonspatial Attributes of Auditory Stimuli in the Ventrolateral Prefrontal Cortex. J Neurosci. 2004; 24(50):11307–11316. https://doi.org/10.1523/JNEUROSCI.3935-04.2004 PMID: 15601937

69. Griffiths TD, Warren JD. What is an auditory object? Nat Rev Neurosci. 2004; 5(11):887–892. https://doi.org/10.1038/nrn1538 PMID: 15496866

70. Rauschecker JP, Scott SK. Maps and streams in the auditory cortex: nonhuman primates illuminate human speech processing. Nat Neurosci. 2009; 12(6):718. https://doi.org/10.1038/nn.2331 PMID: 19471271

71. DeWitt I, Rauschecker JP. Phoneme and word recognition in the auditory ventral stream. PNAS. 2012; 109(8):E505–E514. https://doi.org/10.1073/pnas.1113427109 PMID: 22308358

72. Heald SL, Van Hedger SC, Nusbaum HC. Perceptual plasticity for auditory object recognition. Front Psychol. 2017; 8:781. https://doi.org/10.3389/fpsyg.2017.00781 PMID: 28588524

73. DiCarlo JJ, Zoccolan D, Rust NC. How does the brain solve visual object recognition? Neuron. 2012; 73(3):415–434. https://doi.org/10.1016/j.neuron.2012.01.010 PMID: 22325196

74. Riesenhuber M, Poggio T. Hierarchical models of object recognition in cortex. Nat Neurosci. 1999; 2 (11):1019–1025. https://doi.org/10.1038/14819 PMID: 10526343

75. Wang Y, Markram H, Goodman PH, Berger TK, Ma J, Goldman-Rakic PS. Heterogeneity in the pyramidal network of the medial prefrontal cortex. Nat Neurosci. 2006; 9(4):534–542. https://doi.org/10.1038/nn1670 PMID: 16547512

76. van Aerde KI, Feldmeyer D. Morphological and physiological characterization of pyramidal neuron subtypes in rat medial prefrontal cortex. Cereb Cortex. 2015; 25(3):788–805. https://doi.org/10.1093/cercor/bht278 PMID: 24108807

77. Tasic B, Menon V, Nguyen TN, Kim TK, Jarsky T, Yao Z, et al. Adult mouse cortical cell taxonomy revealed by single cell transcriptomics. Nat Neurosci. 2016; 19(2):335–346. https://doi.org/10.1038/nn.4216 PMID: 26727548

78. Nataraj K, Turrigiano G. Regional and temporal specificity of intrinsic plasticity mechanisms in rodent primary visual cortex. J Neurosci. 2011; 31(49):17932–17940. https://doi.org/10.1523/JNEUROSCI.4455-11.2011 PMID: 22159108

79. Mahon S, Charpier S. Bidirectional plasticity of intrinsic excitability controls sensory inputs efficiency in layer 5 barrel cortex neurons in vivo. J Neurosci. 2012; 32(33):11377–11389. https://doi.org/10.1523/JNEUROSCI.0415-12.2012 PMID: 22895720

80. Dehorter N, Ciceri G, Bartolini G, Lim L, del Pino I, Marin O. Tuning of fast-spiking interneuron properties by an activity-dependent transcriptional switch. Science. 2015; 349(6253):1216–1220. https://doi.org/10.1126/science.aab3415 PMID: 26359400

81. Singh NC, Theunissen FE. Modulation spectra of natural sounds and ethological theories of auditory processing. JASA. 2003; 114(6 Pt 1):3394–3411. https://doi.org/10.1121/1.1624067

82. Gill P, Zhang J, Woolley SMN, Fremouw T, Theunissen FE. Sound representation methods for spectro-temporal receptive field estimation. J Comput Neurosci. 2006; 21(1):5–20. https://doi.org/10.1007/s10827-006-7059-4 PMID: 16633939